Environmental Science and Pollution Research (2019) 26:27888–27896
https://doi.org/10.1007/s11356-019-05847-y

RESEARCH ARTICLE

NO_x adsorption and desorption of a Mn-incorporated NSR catalyst Pt/Ba/Ce/xMn/γ-Al_2O_3

Pan Wang[1] · Dan Yu[1] · Gang Wu[2] · Farhan Sheikh[1] · Junheng Liu[1]

Received: 19 February 2019 / Accepted: 24 June 2019 / Published online: 25 July 2019

Abstract

This study evaluated the NO_x adsorption and desorption performance as well as the casual relationship underlying a Mn-incorporated catalyst (Pt/Ba/Ce/xMn/γ-Al_2O_3). NO_x adsorption and desorption are regarded as a prominent index for the NO_x removal performance of NO_x storage and reduction; we utilized NO_x storage experiments with various inlet NO and O_2 concentrations and cycling adsorption/desorption experiments with a couple of adsorption time protocols for performance evaluation. In-suit DRIFT and NO_x-TPD tests were implemented to reveal the instant stored species and their thermal stability. Eight percent of Mn catalyst at 350 °C was adopted in the described experiments for its desirable NO_x adsorption characteristics. The optimal NO_x storage performance was found under 10% O_2, deteriorating when the concentration was further increased. Furthermore, elevating NO concentration impaired the NO_x adsorption due to the low NO_2/NO_x ratio. It was also found that shorter adsorption time facilitated NO_x removal via maintaining an unsaturated state for active storage components in terms of a fixed desorption time. The stored species existed as nitrites and nitrates with a good low-temperature thermal stability which however decayed at higher temperatures as exhibited in the DRIFT and NO_x-TPD tests. These findings provided invaluable information for the application of Mn-incorporated catalyst for NO_x removal in diesel exhaust purification to relieve the aerial pollution.

Keywords NO_x · NSR · Adsorption/desorption · NO_x-TPD · NO_x storage efficiency

Introduction

The global quest for safer environment as well as continuous agitation for the reduction of global warming has initiated more stringent emission regulatory demands especially towards the reduction of NO_x which are considered as heavy air pollutants (Ting et al. 2018). It is therefore of great necessity to develop and apply novel and more advanced post-treatment technologies for the removal of NO_x emissions especially for diesel engines which are known for higher fuel efficiency and lower greenhouse gas emission, but NO_x reduction is more difficult to achieve due to excessive supply of oxygen during combustion (Sim et al. 2014).

In order to solve this drawback, the NO_x storage and reduction (NSR) technology has been employed as one of the most promising and recognized methods (Constantinou et al. 2013; Ji et al. 2015). It has an excellent NO_x removal performance under lean fuel condition and at low temperature (Constantinou et al. 2013; Ji et al. 2015). The NSR functions through the storage of NO_x as nitrites and nitrates during regular lean conditions and is further reduced to N_2 in the short rich periods (Du et al. 2018; Shakya et al. 2012). The NSR catalyst consists of a noble metal component, a storage component, and a support (Roy and Baiker 2008), among which Pt/Ba/γ-Al_2O_3 is currently known for its widespread use (Xu et al. 2016). Although γ-Al_2O_3 has been extensively utilized as a support component of the NSR catalyst, a number of disadvantages have accompanied its usage including sintering, phase changes at high temperatures, and inferior

Responsible editor: Philippe Garrigues

✉ Pan Wang
wangpan@ujs.edu.cn

✉ Gang Wu
wug1999@163.com

[1] School of Automotive and Traffic Engineering, Jiangsu University, Zhenjiang 212013, China

[2] College of Automotive and Mechanical Engineering, Changsha University of Science and Technology, Yuhua District, Changsha City 410114, Hunan, China

anti-sulfur capacity (Huang et al. 2013). Noble metal is a very fundamental component of the NSR due to its irreplaceable role in the NO_x storage and reduction, despite its low level in the NSR catalyst (Gonzalez-Marcos et al. 2013).

Previous studies (Sim et al. 2014; Ryou et al. 2018) have shown that platinum (Pt) is easily deactivated due to its sintering effect at high temperatures albeit being the most effective noble metal when compared with palladium (Pd) and rhodium (Rh) with a relatively lower cost and better storage characteristics. Barium (Ba) is one of the alkaline-earth metals widely employed as storage component and it is widely utilized due to its superior storage capacity and NO_x desorption in contrast to Sr, Ca, and K; however, due to its poor anti-sulfur ability, barium oxide (BaO) reacts with sulfur dioxide (SO_2) and Pt within the lean and rich fuel conditions, generating $BaSO_4$ and PtS, respectively, which is detrimental to catalytic activity (Nguyena et al. 2018; Yang et al. 2014; Corbos et al. 2008). Therefore, improvements on these drawbacks are urgently needed in order to perfect catalytic properties and efficiency.

The reactivity of the NSR catalyst is greatly influenced by the interaction between the three components of the NSR catalyst (noble metal components, storage components, and support). MnO_x, CeO_x, and CoO_x acts on elevating the NO_x storage capacity and anti-sulfur ability (Bai et al. 2017; Wang et al. 2017), while CeO_2 enhances the removal of NO_x by facilitating hydrocarbon reforming and water-gas shift (WGS) reactions (Wang et al. 2011). Some studies (Ji et al. 2018; Xiao et al. 2008; Tang et al. 2006) have demonstrated that Mn significantly improved the oxidation of NO to NO_2, thus facilitating the storage and removal of NO_x. Furthermore, it has been reported that Pd/Mn/Ba/Al catalytic system displayed a stronger NO oxidation and NO_x removal capability than Pd/Ba/Al, suggesting the function of Mn in the reduction of NO_x in NSR catalyst (Zhang et al. 2015). Notably, the inhibitory effect of H_2O and CO_2 on NO_x adsorption and desorption can be alleviated by Mn as a result of the decomposition of $MnCO_3$ at low temperature (Guo et al. 2009). Therefore, the application of a Pt/Ce/Ba/γ-Al_2O_3 catalyst which incorporates Mn would be a suitable and promising catalytic model for the removal of NO_x.

To the best of our knowledge, the conversion of NO to NO_2 is beneficial to NO_x storage as NO_2 is readily stored. Thus, NO conversion is significantly influenced by the dosages of NO and O_2 as well as the adsorption time. An increase of NO and O_2 has been suggested to facilitate the generation of more stable nitrates based on the fact that NO adsorption would proceed as a result of the weak bond between surface oxygen species and Mn (Liang et al., 2017; Guo et al. 2017). Besides, NO_x storage/reduction performance has been reported to be closely related to temperature, since NO oxidation is retarded at low temperature and stored species would decompose at relatively high temperature (Andonova et al. 2017; Liu et al. 2017).

Despite the advantages of Mn as a component of NSR catalysts, the effect of internal/external factors on the NO_x removal performance as well as the NO_x adsorption and desorption mechanism under various conditions has not been fully understood and explored and thus requires further investigation. In this study, the NO_x adsorption and desorption characteristics were investigated as a function of various NO and O_2 concentrations, temperature, and storage time in order to investigate the NO_x adsorption/desorption performance over a Mn-incorporated NSR catalyst (Pt/15Ba/15Ce/xMn/γ-Al_2O_3). These findings combined with in-suit DRIFT and NO_x-TPD results carry a thorough and profound implication for the NO_x adsorption and desorption performance over Mn-incorporated NSR catalysts and potential application in advanced post-treatment technology.

Experimental

Catalyst preparation

The NSR catalyst Pt/15Ba/15Ce/xMn/γ-Al_2O_3 was prepared as follows.

Ba, Ce, and Mn nanoparticles were deposited onto γ-Al_2O_3 by the sol-gel method. Briefly, a so-gel solution was prepared by dissolving stoichiometric ratio of barium acetate, cerium acetate, and manganese acetate aqueous solution into γ-Al_2O_3 turbid liquid, followed by the addition of citric acid and polyethylene glycol at 80 °C under continuous stirring. The reaction solution was dried at 110 °C for 24 h and calcined at 500 °C for 5 h in the muffle furnace. Pt was incorporated using a wetness impregnation method. The Ba/Ce/Mn/γ-Al_2O_3 sample was impregnated with an aqueous solution of chloroplatinic acid, dried at 110 °C for 24 h, and calcined at 500 °C for 5 h. The different Mn loadings (6, 8, and 10 wt.%) were loaded using the same method.

In-suit DRIFT and NO_x-TPD tests

The in-suit DRIFT test was performed on a Nicolet 6700 (Thermo Fisher Scientific) at a wavelength range of 400–4000 cm^{-1} with 32 scans. Before the test, pretreatment was conducted by flushing the sample with nitrogen at 450 °C for 45 min. The spectrum was recorded during NO adsorption (500 ppm NO, 10% O_2 and N_2) consecutively for 30 min. The thermal stability of the adsorbed NO_x species was measured using NO_x temperature-programmed desorption (TPD) carried out on a two-zone furnace. The NO_x adsorption was conducted at temperature from 100 to 450 °C and kept at 450 °C in 500 ppm NO, 10% O_2, and balance N_2 for some period of time. After cooling down the temperature of the

sample to 100 °C, the catalysts was heated from 100 to 600 °C in a linear temperature ramp of 10 °C/min within N_2.

Catalyst performance evaluation through a reactor system

The catalyst performance as the function of different parameters was carried out through a continuous flow quartz reactor as previously described in the literature (Ji et al. 2017). The catalyst powder was sustained with quartz wool in a reactor tube with an inner diameter of 7 mm. Four gas cylinders and a mass flow controller enabled the simulation of the composition and concentrations of various gas components for the supplied gas model. An electric furnace was used to control the reaction temperature. The NO_x concentration was determined by a specific Fourier transform infrared spectroscope (FTIR) with the help of a combination of analysis software. All flow conditions were operated at a gas hourly space velocity (GHSV) of 52,000 h^{-1} and a total flow rate of 30 mL/min. The catalyst was pretreated at 450 °C for 1 h in a feedstream composed of 1% H_2 in N_2 so as to ascertain the purity of the catalyst.

The lean feed consisting of 500 ppm NO, 10% O_2, and N_2 as balance gas was introduced into the reactor and adsorbed until saturated in NO_x storage experiments. Alteration of the temperature and reaction atmosphere was allowed in order to evaluate its impacts on various parameters. The significance of NO and O_2 during the NO_x adsorption and desorption was investigated by NO_x storage experiments at 350 °C with various inlet O_2 (0, 5, 10, and 15%) and NO (500, 700, and 1000 ppm) concentrations. A fixed NO concentration of 500 ppm was employed for the evaluation of O_2 effect, while 10% was used for NO effect. The cycling storage/reduction experiment was performed using different time protocols of 60 s/60 s, 120 s/60 s, and 180 s/60 s (lean/rich or adsorption/desorption) employing a rich feed composed of 1% H_2 in N_2 which was admitted after a time-restricted adsorption.

The NO_x storage capacity and NO_x storage efficiency are computed using the following formulae which act as an index of NO_x adsorption/desorption performance:

$$\mathrm{NSC} = \frac{\left(\mathrm{F}_{\mathrm{NOx}}^{\mathrm{inlet}} t_L - \int_0^{t_L} \mathrm{F}_{\mathrm{NOx}}^{\mathrm{outlet}} dt\right) \times v}{V \times m} \tag{1}$$

$$\eta_{\mathrm{NO_x}} = \frac{\mathrm{F}_{\mathrm{NOx}}^{\mathrm{inlet}} t_L - \int_0^{t_L} \mathrm{F}_{\mathrm{NOx}}^{\mathrm{outlet}} dt}{\mathrm{F}_{\mathrm{NOx}}^{\mathrm{inlet}} t_L} \times 100\% \tag{2}$$

where $\mathrm{F}_{\mathrm{NO_x}}^{\mathrm{inlet}}$ and $\mathrm{F}_{\mathrm{NO_x}}^{\mathrm{outlet}}$ represent the NO_x concentration at the inlet (500 ppm) and outlet; t_L denotes the storage time (s); m is the catalyst mass (g); and V is the molar volume of gas taken as 22.4 mol/L.

The average NO_2/NO_x ratio is defined with the formula below:

$$R_{\mathrm{NO_2/NOx}} = \frac{\int_0^{t_L} \mathrm{F}_{\mathrm{NO_2}}^{\mathrm{outlet}} t_L dt}{\int_0^{t_L} \mathrm{F}_{\mathrm{NOx}}^{\mathrm{outlet}} t_L dt} \times 100\% \tag{3}$$

where $\mathrm{F}_{\mathrm{NO_x}}^{\mathrm{outlet}}$ and $\mathrm{F}_{\mathrm{NO_2}}^{\mathrm{outlet}}$ represent the NO_x and NO_2 concentrations at the outlet; and t_L denotes the storage time (s).

Results and discussion

Performance evaluation in temperature experiment

The effect of temperature was evaluated via NO_x storage experiment. Figure 1a illustrates a lucid comparison of the storage efficiency for the Mn-incorporated catalyst with 6%, 8%, and 10% Mn loading. As clearly seen, 8% Mn-incorporated catalyst displayed a higher storage efficiency at 350 °C as compared with 6% and 10% Mn loadings. Therefore, the catalyst with 8% Mn loading was tested on its adsorption performance under various temperatures so as to obtain a deeper understanding of the mechanism involved in NO_x storage and reduction.

As shown in Fig. 1b, the outlet NO_x yield was almost not detected during the first few minutes indicating a desirable adsorption. Specifically, the breakthrough time and saturation time were defined as the time required for NO_x to be detected and get saturated within the effluent, respectively; longer duration is representative of better NO_x storage performance. It was observed that the breakthrough time increased with increase in temperature from 250 to 350 °C, while a downward trend was observed as the temperature was further increased to 450 °C. The saturation time was also observed to follow the same trend as the temperature was increased as shown in Table 1.

The NO_x storage efficiency of 8% Mn catalyst described in Fig. 1a was also validated based on the results obtained from the foregoing breakthrough time and saturation time; the 8% Mn catalyst displayed the best adsorption characteristic at 350 °C. This may be probably caused by the inhibition of NO oxidation at low temperature like 250 °C and the thermal stability decay of stored species (such as nitrites and nitrates) surpassing the enhancement of catalytic reactivity at high temperature like 450 °C. As a result, 8% Mn catalyst was tested upon its adsorption and desorption performance at 350 °C in the experiments illustrated below.

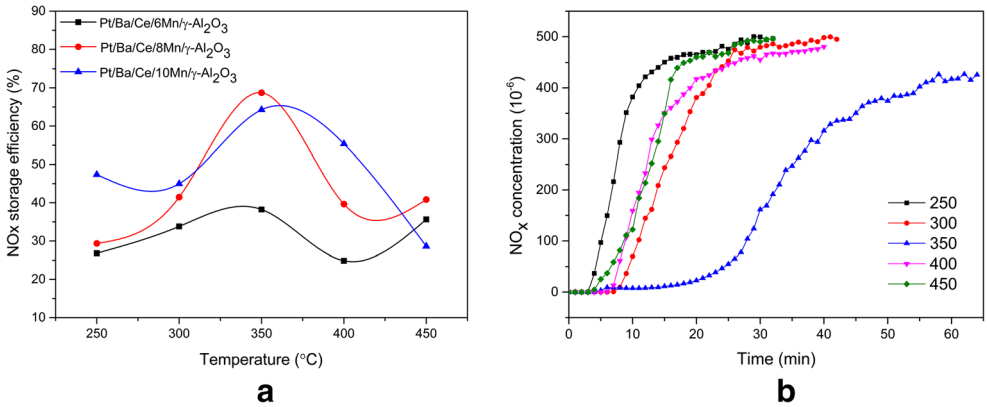

Fig. 1 **a** NO_x storage efficiency of the target Mn-containing catalyst at various temperatures. (**b**) NO_x adsorption performance of 8% Mn catalysts at different temperatures

Performance evaluation under various O_2 concentrations

The effect of the concentration of O_2 investigated in NO_x storage experiments as well as its impacts on NO_x adsorption is shown in Fig. 2. The results with 0% O_2 in Fig. 2a were twofold. NO_2 was not observed throughout the whole storage process and outlet NO_x yield surged during the first 10 min; the former suggested the absence of NO oxidation while the latter implied inferior NO_x storage performance. Table 2 provides a systematic analysis on the comparison of NO_x adsorption performance in the presence of varying O_2 concentrations. The NO_x storage curves (observed in Figs. 1b and 2b) became those typical ones as analyzed in the "Performance evaluation in temperature experiment" section once O_2 was admitted and ascribed to NO_2 oxidization by NO in an atmosphere containing O_2. As clearly observed, NO_2/NO_x ratio was low at 5% O_2 but higher with increased O_2 concentration. At 10% O_2 concentration, an optimal adsorption capacity of 690 μmol/g_{cat} was achieved as compared with 15% O_2 where the adsorption capacity was only 450 μmol/g_{cat} (Table 2). Figure 2c illustrates the storage efficiency of NO_x as a function of time; NO_x storage efficiency reduced with time and enhanced with increasing O_2 concentration until 10% O_2 was achieved. The storage efficiency under 10% O_2 was sustained at a relatively high level (above 95%) over the first 20 min but decreased as the concentration of O_2 was increased to 15%. Furthermore, the results indicated that O_2 is essential for NO_x storage for its function to increase the NO_2/NO_x ratio within a certain range facilitating NO_x storage, since NO_2 acts as the main force in the NO_x adsorption as nitrites and nitrates, whereas the poor storage capacity at 15% O_2 might majorly be caused by superfluous NO_2, which could not be adsorbed by limited active sites in spite of the increase in average NO_2/NO_x ratio from 48 to 50% (Table 2). The adsorption mechanism could be explained with the help of the following reactions:

$$2NO + O_2 \rightarrow 2NO_2 \quad (4)$$

$$BaCO_3 + 2NO + 3/2O_2 \rightarrow Ba(NO_3)_2 + CO_2 \quad (5)$$

$$BaCO_3 + 3NO_2 \rightarrow Ba(NO_3)_2 + NO \quad (6)$$

Similar experiments were carried out with 8% O_2 (Zhang et al. 2015); a NO_x storage capacity of 255.4 μmol/g_{cat} was also found over $5Mn/10Ba/Al_2O_3$ catalyst according to (Zhang et al. 2017), which is less than half of 690 μmol/g_{cat} over $Pt/15Ba/15Ce/10Mn/Al_2O_3$ catalyst, as shown in Table 2. It indicated that the components Pt and Ce remarkably promoted the NO_x storage capacity over NSR catalyst.

Table 1 Breakthrough time and saturation time for 8% Mn loading under various temperatures

Temperature (°C)	Breakthrough time (min)	Saturation time (min)
250	3	34
300	4	43
350	6	70
400	4	44
450	3	35

Performance evaluation under various NO concentrations

Figure 3 compares the NO_x storage performance over $Pt/Ba/Ce/8Mn/\gamma\text{-}Al_2O_3$ at 10% O_2 and at various NO concentrations. It was observed that the outlet NO_x yield and the growth rate were both enhanced when inlet NO proportion was increased from 500 to 1000 ppm. This finding suggested an inhibition of the NO_x storage process as supported by a decline in the breakthrough time from 8 to 2.5 min, saturation time from 64 to 36 min (Fig. 3), NO_x storage capacity from 690 to 418 μmol/g_{cat}, and NO_x storage efficiency from 64 to 31% (Table 3). These may be as a result of the decrease in NO_2/NO_x ratio from 48 to 36% in average with NO concentration from 500 to 1000 ppm, as visibly illustrated in Table 3. There are two possible reasons for the decreased NO_2/NO_x

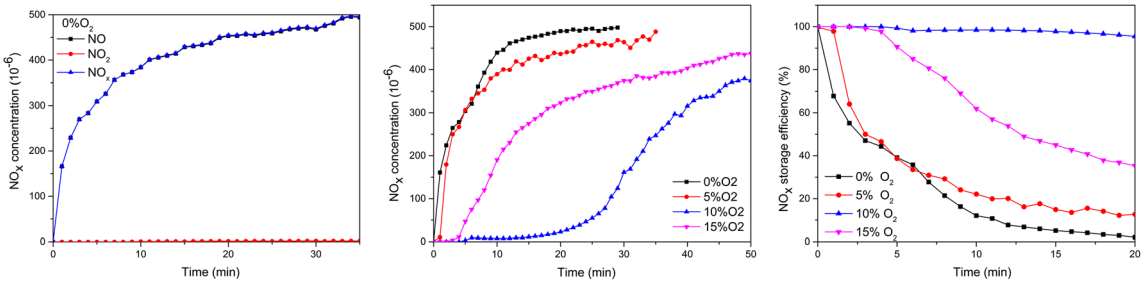

Fig. 2 Comparison of outlet NO_x concentrations (**b**) and NO_x storage efficiency (**c**) as a function of time with 0% (**a**), 5%, 10%, and 15% O_2 via NO_x storage experiments at 350 °C

ratio; the oxidizing capability of the active storage components, such as Mn and Ce, may not be able to sustain the excessive amount of NO, resulting in the exhaustion of NO at the effluents. In spite of the increase in NO_2 oxidation from NO, the NO_2 storage as nitrates was limited by a limited amount of active sites on the catalyst surface as stated in the "Performance evaluation under various O_2 concentrations" section. Therefore, an increase in NO concentration would impair NO_x storage and NO_x removal by downregulating the NO_2 proportion in NO_x. As shown in Fig. 3d, for the NO_x storage efficiency at 500 ppm, NO remained high after 40 min at about 80% and was much higher and steadier when compared with the NO_x storage efficiency at 750 ppm and 1000 ppm. This results suggest that 500 ppm NO would produce an excellent NO_x storage performance.

Effect of adsorption time on NO_x adsorption/desorption

In order to investigate the effect imposed by adsorption time on catalytic performance, 10% O_2 and 500 ppm NO were utilized in the cycling storage/reduction experiments with different adsorption time protocols as displayed in Fig. 4. A peak yield of NO_x occurred when H_2 was introduced into the reactor, which was attributed to the decomposition of stored species and their further aggravation as a result of the heat generated during the reduction. It was observed that the peak yield of NO_x kept increasing until a steady state was achieved at the start of the cycles and the stable peak also increased when the adsorption time increased from 60 to 180 s, indicating excess NO spilling-off due to limited active storage sites (Table 4). The steady value of NO_x concentration was also found to increase when the adsorption time was increased, which implied an unsaturated storage under an adsorption time of 60 s, 120 s, and probably 180 s. Notably at the beginning of storage, NO_2 split off prior to NO, suggesting an excellent oxidation capability of Mn to convert NO into NO_2.

Table 4 elaborated the NO_x storage and removal performance by providing a quantitative analysis. As observed, the NO_x storage and removal efficiency both exceeded 70%, implying favorable catalyst characteristics of Pt/15Ba/15Ce/8Mn/γ-Al_2O_3. However, the NO_x removal performance decreased as the adsorption time increased. An optimal NO_x desorption efficiency occurred at an adsorption time of 60 s; however, the NO_x desorption efficiency was decreased from 82 to 75% when the adsorption time was increased from 60 to 180 s. This may possibly be due to the alleviation of adsorption burden as a result of low concentration/proportion of NO_2 in the limited active sites which could be kept in a smooth working state without saturation under a shorter adsorption time. Interestingly, the desorption peak was increased from 153 to 226 ppm, which was probably due to the presence of a major part of NO in the desorption peak during the NO_x storage and reduction. These results were quite the opposite under longer duration of adsorption time. A large amount of NO_x was discharged directly without storage, resulting in higher NO_x emission and lower NO_x removal efficiency. Therefore, it is reasonable to suggest that a relatively shorter adsorption time (under a specific desorption time) is essential for the enhancement of NO_x removal performance.

Table 2 Related parameters upon NO_x storage performance with various O_2 concentrations

O_2 concentration (%)	NO_x storage efficiency (%)	NO_x storage capacity ($\mu mol/g_{cat}$)	Average NO_2/NO_x ratio (%)	Breakthrough time (min)	Saturation time (min)
0	18	115	0	1	29
5	23	167	37	2	34
10	90	690	48	9	64
15	40	450	50	4	50

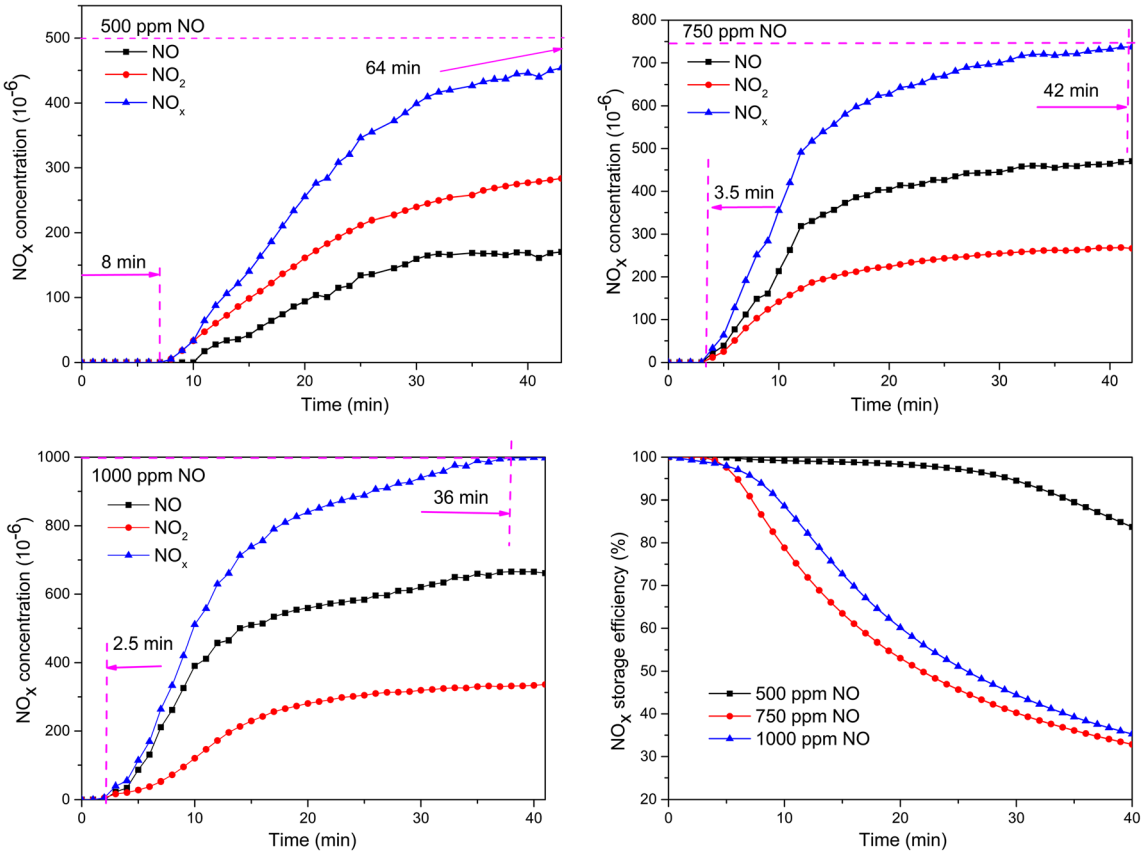

Fig. 3 Comparison of outlet NO_x yields with 500 (**a**), 750 (**b**), and 1000 (**c**) ppm NO and their NO_x storage efficiency (**d**) in NO_x storage experiments at 350 °C

In-suit DRIFT and NO_x-TPD results

An in-suit DRIFT test was performed at 250 °C to provide an insight into the intermediate species formed during the NO_x adsorption. A spectra of absorbance against time was obtained as shown in Fig. 5. The spectra exhibited various absorption bands at 1122, 1250, 1332, 1530, 1624, and 1762 cm^{-1}, and NO_2^- adsorption peaks were observed at 1380–1320 cm^{-1}, 1250–1230 cm^{-1}, and 840–800 cm^{-1}, while NO_3^- was observed at 1380–1350 cm^{-1} and 840–815 cm^{-1} according to previous literature (Zheng et al. 2017; Say et al. 2016). Accordingly, the peaks in Fig. 5 correspond to a variety of nitrogen oxide species, including bidentate nitrate (1122 cm^{-1}), nitrate adsorbed on Ba (1332 cm^{-1}), and bridging nitro-nitrito (1624 cm^{-1}). Notably, an adsorption peak of N_2O_4 was also observed at 1762 cm^{-1}. From the transformation of stored species, it was observed that NO_x was initially stored as nitrites (1122 cm^{-1}) and then together with nitrate peaks as the intensity of nitrite peaks increased, thus suggesting that the stored species were mostly in the form of nitrites and partly as nitrates. Interestingly, the occurrence of nitrates at 250 °C conflicted with the findings in literatures (Castoldia et al. 2018). It was assumed that the incorporation of Mn and Ce into the NSR catalyst facilitated the oxidization of NO_x species to stable nitrates at low temperature, promoting the NO_x adsorption.

A desorption curve as a function of temperature in Fig. 6 was obtained via the NO_x-TPD technology as a means of elucidating the thermal stability of the catalyst. It is clearly observed that the major NO_x species desorped were NO and NO_2, and the desorption peaks were found around 580 ppm at 450 °C and 60 ppm at 380 °C, respectively. Interestingly, the

Table 3 Related parameters of NO_x storage performance with various NO concentrations

NO concentration (10^{-6} *v/v*)	NO_x storage efficiency (%)	NO_x storage capacity ($\mu mol/g_{cat}$)	Average NO_2/NO_x ratio (%)	Breakthrough time (min)	Saturation time (min)
500	64	690	48	8	64
750	36	517	39	3.5	42
1000	31	418	36	2.5	36

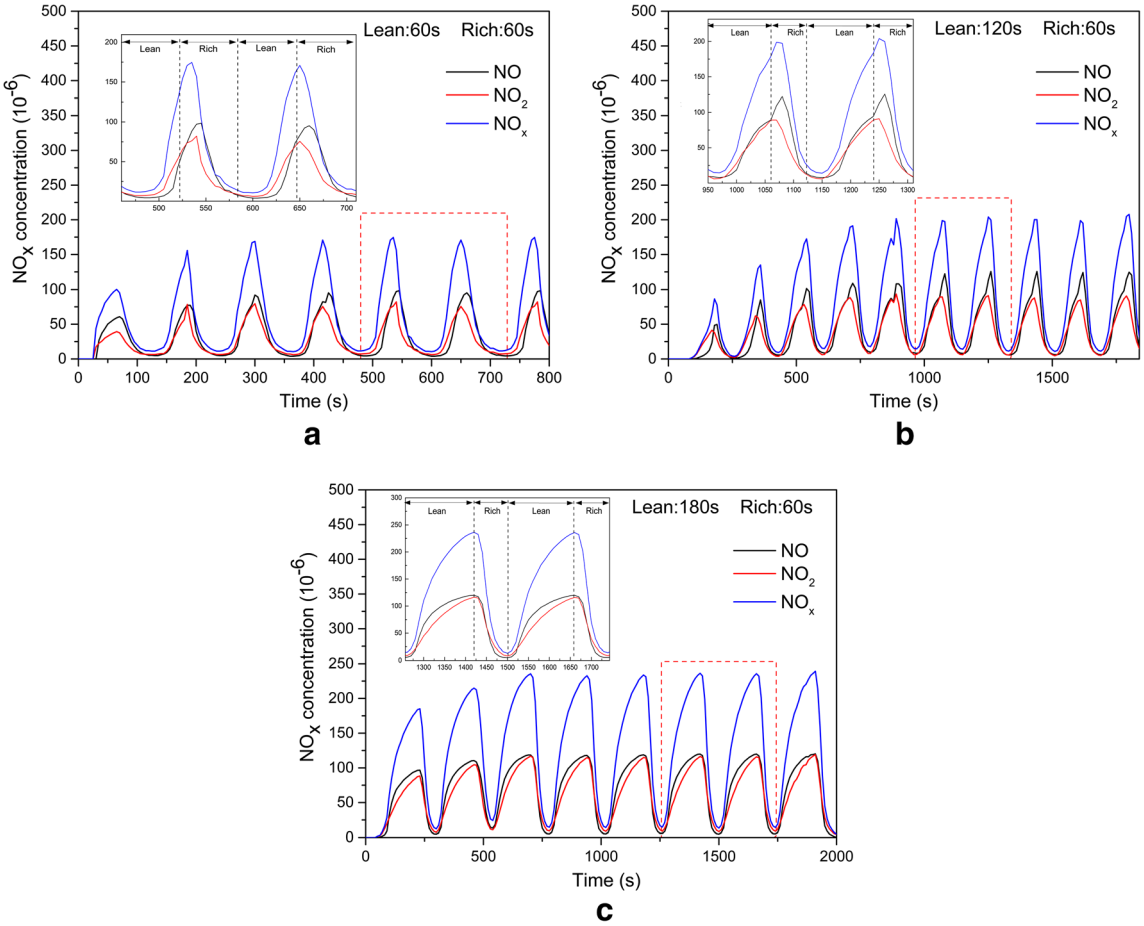

Fig. 4 Impact of adsorption time on NO_x storage and reduction with duration of 60 s (**a**), 120 s (**b**), and 180 s (**c**) for storage and 60 s for reduction

temperature of NO exceeded that of NO_2 by 70 °C at the desorption peak, suggesting a better thermal stability for nitrites; and NO_2 desorption was rather lower than NO, at least partly attributed to NO being favored compared with NO_2 during the thermal dynamic equilibrium at high temperature. It is noteworthy to say that the catalyst oxidizing ability could get enhanced at higher temperature promoting NO_2 generation and the conversion of Mn to Mn^{3+} and Mn^{4+} at high temperature also contributed to the oxidation of NO to NO_2, thus facilitating NO_x storage as nitrites and nitrates. It is assumed that the adsorption of NO_2 was weakened and eventually terminated after 380 °C due to the increase in oxygen consumption stored on storage components Ba and Ce. Due to the thermometric impact, NO_x (NO and NO_2) desorption began at around 300 °C and declined due to temperature elevation after the desorption peak, suggesting fine and weaken thermal stability at low temperature and higher temperature, respectively. Presumably, the NO desorption peak at 450 °C was induced by nitrite and nitrate decomposition and NO_2 adsorption and desorption were inhibited by the absence of stored oxygen to oxidize NO at high temperature. It could be deduced that NO_x desorption arose from the weak bond between stored species and the active sites at low temperature and decomposition of stored nitrites and nitrates at high temperature, which is in line with the literature (Tamm et al. 2014). Evidently, a favorable thermal stability was achieved at low

Table 4 Related parameters on NO_x storage and reduction performance at different time protocols

Lean/rich periods (s)	NO_x storage efficiency (%)	Desorption peak ($\times 10^{-6}$ *v/v*)	NO_x storage capacity (μmol/g_{cat})	NO_x removal efficiency (%)
60/60	87	153	58	82
120/60	83	182	56	82
180/60	72	226	59	75

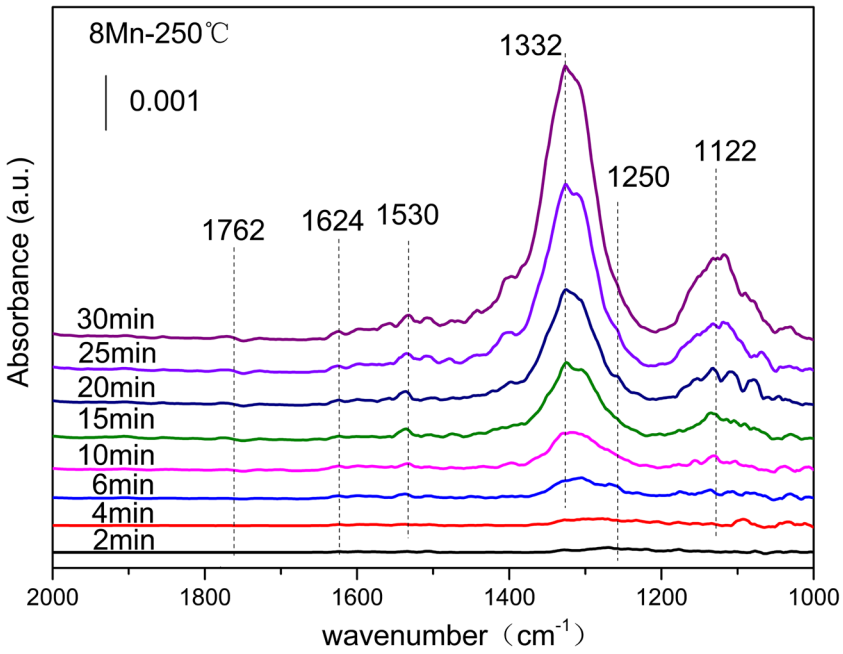

Fig. 5 DRIFT spectra of Pt/15Ba/15Ce/8Mn/γ-Al_2O_3 catalyst at 250 °C

temperature, deteriorating at higher temperature which would assist in explaining the results in Fig. 1b. The desorption mechanism at high temperature can be illustrated by the following equations:

$$Ba(NO_2)_2 \rightarrow BaO + 2NO + 1/2O_2 \quad (7)$$

$$Ba(NO_3)_2 \rightarrow BaO + 2NO + 3/2O_2 \quad (8)$$

$$Ba(NO_3)_2 \rightarrow BaO + 2NO_2 + O_2 \quad (9)$$

Conclusions

This study provides a deeper insight into the NO_x adsorption and desorption performance as well as the underlying mechanism. The temperature experiments indicated that Pt/15Ba/15Ce/8Mn/γ-Al_2O_3 presented a satisfactory NO_x adsorption performance at 350 °C. Under various NO and O_2 concentrations in the NO_x storage experiments, the NO_x adsorption performance was found to be optimal under 10% O_2 in this study and was decreased when O_2 concentration was further increased owing to the surplus NO_2 and limited active sites. In addition, elevation of NO concentration impaired the NO_x adsorption probably due to

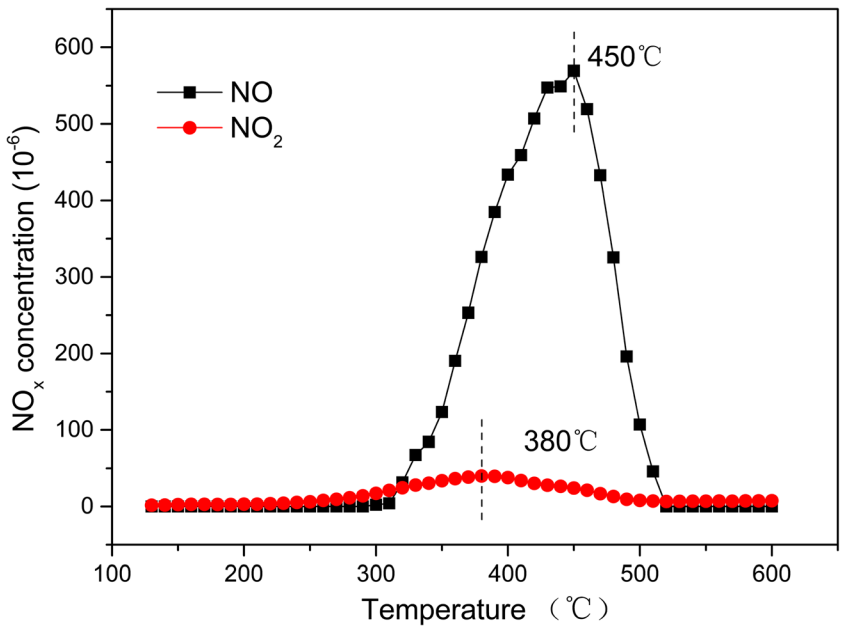

Fig. 6 NO_x desorption curves as a function of temperature in NO_x-TPD experiments

the low NO_2/NO_x ratio. The results obtained from the cycling NO_x storage/reduction experiment showed priority to the shorter adsorption time for NO_x removal as it could help maintain an unsaturated state over active storage components. Notably, the stored species existed mainly as nitrites and partly nitrates at 250 °C in the DRIFT measurements implying that Mn facilitated the oxidation of NO_x species to stable nitrates at a low temperature. NO_x-TPD experiments demonstrated that the stored species displayed excellent low-temperature thermal stability promoted probably by Mn, albeit the degradation arising from decomposition of stored nitrites and nitrates at high temperature.

Acknowledgments The authors acknowledge the contribution of Professor Guanjun Qiao for the technical supports.

Funding information This project was funded by the National Natural Science Foundation of China (No. 51676090), Natural Science Foundation of Jiangsu Province (No. BK20150513), and the Six Talent Peaks Project in Jiangsu Province.

References

Andonova S, Marchionni V, Lietti L et al (2017) Micro-calorimetric studies of NO_2 adsorption on Pt/BaO supported on γ-Al_2O_3 NO_x storage and reduction (NSR) catalysts impact of CO_2. Mol Catal 436:43–52

Bai Z, Zhang Z, Chen B, Zhao Q, Crocker M, Shi C (2017) Non-thermal plasma enhanced NSR performance over Pt/M/Ba/Al_2O_3 (M=Mn, Co, Cu) catalysts. Chem Eng J 314:688–699

Castoldia L, Matarresea R, Morandi S (2018) New insights on the adsorption, thermal decomposition and reduction of NO_x over Pt- and Ba-based catalysts. Appl Catal B Environ 224:249–263

Constantinou C, Li W, Qi G, Epling WS (2013) NO_x storage and reduction over a perovskite-based lean NOx trap catalyst. Appl Catal B Environ 134-135:66–74

Corbos EC, Courtois X, Bion N, Marecot P, Duprez D (2008) Impact of the support oxide and Ba loading on the sulfur resistance and regeneration of Pt/Ba/support catalysts. Appl Catal B Environ 80(1–2):62–71

Du SC, Wang SB, Guo YB et al (2018) Rational design, synthesis and evaluation of ZnO nanorod array supported Pt: $La_{0.8}Sr_{0.2}MnO_3$ lean NO_x traps. Appl Catal B Environ 236:348–358

Gonzalez-Marcos MP, Pereda B, Torre UDL, Gonzalez-Velasco JR (2013) On the effect of reduction and ageing on the TWC activity of Pt/$Ce_{0.68}Zr_{0.32}O_2$ under simulated automotive exhausts. Top Catal 56:352–357

Guo H, Li X, Wang Z (2009) Preparation of manganese oxide with high density by decomposition of $MnCO_3$ and its application to synthesis of $LiMn_2O_4$. J Power Sources 189:95–100

Guo LH, Guo L, Zhao DY, Gao ZN, Tian Y, Ding T, Zhang J, Zheng LR, Li XG (2017) Oxidizing, trapping and releasing NO_x over model manganese oxides in alternative lean-burn/fuel-rich atmospheres at low temperatures. Catal Today 297:27–35

Huang B, Bartholomew CH, Smith SJ, Woodfield BF (2013) Facile solvent-deficient synthesis of mesoporous γ-alumina with controlled pore structures. Microporous Mesoporous Mater 165:70–78

Ji Y, Bai S, Crocker M et al (2015) Al_2O_3-based passive NO_x adsorbers for low temperature applications. Appl Catal B Environ 170-171:283–292

Ji Y, Xu D, Bai S et al (2017) Pt- and Pd-promoted CeO_2–ZrO_2 for passive NO_x adsorber applications. Ind Eng Chem Res 56:111–125

Ji Y, Xu D, Crocker M, Theis JR, Lambert C, Bueno-Lopez A, Harris D, Scapens D (2018) Mn-based mixed oxides for low temperature NO_x adsorber applications. Appl Catal A Gen 567:90–101

Liang YL, Huang YF, Zhang HL et al (2017) Interactional effect of cerium and manganese on NO catalytic oxidation. Environ Sci Pollut Res 24:9314–9324

Liu Y, Guo L, Zhao D, Li X, Gao Z, Ding T, Tian Y, Jiang Z (2017) Enhanced activity of $CuO/K_2CO_3/MgAl_2O_4$ catalyst for lean NOx storage and reduction at high temperatures. RSC Adv 7:27405–27414

Nguyena HP, Valle SPD, Marie O et al (2018) NO_x adsorption on K and Ba loaded on zirconia-titania NSR catalysts: a comparative study by in situ and operando IR spectroscopy. Appl Catal B Environ 231:391–399

Roy S, Baiker A (2008) NO_x storage-reduction catalysis: from mechanism and materials properties to storage-reduction performance. Chem Rev 109:4054–4091

Ryou YS, Lee J, Lee H (2018) Low temperature NO adsorption over hydrothermally aged Pd/CeO_2 for cold start application. Catal Today 307:93–101

Say Z, Tohumeken M, Ozensoy E (2016) Spectroscopic investigation of sulfur-resistant Pt/$K_2O/ZrO_2/TiO_2/Al_2O_3$ NSR/LNT catalysts. Catal Today 267:167–176

Shakya BM, Harold MP, Balakotaiah V (2012) Crystallite-scale model for NO_x storage and reduction on Pt/BaO/Al_2O_3: Pt dispersion effects on NO_x conversion and ammonia selectivity. Catal Today 184:27–42

Sim JS, Gong MJ, Chang KS (2014) Preliminary performance studies of Al–Co–Mn mixed oxide and Ag-doping for the purpose of PGM-free DOC. Appl Catal A Gen 480:120–127

Tamm S, Andonova S, Olsson L (2014) The effect of hydrogen on the storage of NO_x over silver, platinum and barium containing NSR catalysts. Catal Lett 144:1101–1112

Tang XF, Li YG, Huang XM et al (2006) MnO_x–CeO_2 mixed oxide catalysts for complete oxidation of formaldehyde: effect of preparation method and calcination temperature. Appl Catal B Environ 64:265–273

Ting AWL, Harold MP, Balakotaiah V (2018) Elucidating the mechanism of fast cycling NO_x storage and reduction using C_3H_6 and H_2 as reductants. Chem Eng Sci 189:413–421

Wang X, Yu Y, He H (2011) Effects of temperature and reductant type on the process of NO_x storage reduction over Pt/Ba/CeO_2 catalysts. Appl Catal B Environ 104(1–2):151–160

Wang P, Yi J, Gu W, Luo P, Lei LL (2017) The influence of xMnyCe/γ-Al_2O_3 on NO_x catalysts on the properties of NO_x storage and reduction over Pt-Ce-Ba/γ-Al_2O_3 catalysts. Chem Eng J 325:700–707

Xiao J, Li X, Deng S, Wang F, Wang L (2008) NO_x storage-reduction over combined catalyst Mn/Ba/Al_2O_3–Pt/Ba/Al_2O_3. Catal Commun 9:563–567

Xu J, Ibrahim AR, Hu X, Hong Y, Su Y, Wang H, Li J (2016) Preparation of large pore volume γ-alumina and its performance as catalyst support in phenol hydroxylation. Microporous Mesoporous Mater 231:1–8

Yang L, Lin S, Yang X, Fang W, Zhou R (2014) Promoting effect of alkaline earth metal doping on catalytic activity of HC and NO_x conversion over Pd-only three-way catalyst. J Hazard Mater 279:226–235

Zhang ZS, Chen BB, Wang XK, Xu L, Au C, Shi C, Crocker M (2015) NO_x storage and reduction properties of model manganese-based lean NO_x trap catalysts. Appl Catal B Environ 165:232–244

Zhang Z, Crocker M, Chen B et al (2017) Pt-free, non-thermal plasma-assisted NO_x storage and reduction over M/Ba/Al_2O_3 (M = Mn, Fe, Co, Ni, Cu) catalysts. Catal Today 256:115–123

Zheng Y, Kovarik L, Engelhard MH, Wang Y, Wang Y, Gao F, Szanyi J (2017) Low-temperature Pd/zeolite passive NO_x adsorbers: structure, performance and adsorption chemistry. J Phys Chem C 121:15793–15803